Geophysical Research Letters

RESEARCH LETTER
10.1029/2020GL088540

Statistical Properties of Magnetic Structures and Energy Dissipation during Turbulent Reconnection in the Earth's Magnetotail

K. Bergstedt[1,2], H. Ji[1,2], J. Jara-Almonte[2], J. Yoo[2], R. E. Ergun[3,4], and L.-J. Chen[5]

[1]Department of Astrophysical Sciences, Princeton University, Princeton, NJ, USA, [2]Princeton Plasma Physics Laboratory, Princeton, NJ, USA, [3]Department of Astrophysical and Planetary Sciences, University of Colorado Boulder, Boulder, CO, USA, [4]Laboratory of Atmospheric and Space Sciences, University of Colorado Boulder, Boulder, CO, USA, [5]NASA, Goddard Space Flight Center, Greenbelt, MD, USA

Key Points:

- An automated method to locate and identify plasmoids and current sheets in turbulent magnetotail reconnection regions has been developed
- Plasmoids in a region of turbulent magnetotail reconnection have a decaying exponential size distribution from subelectron to ion scale
- Plasmoids and current sheets are significant contributors to parallel particle energization, but not to overall particle energization

Correspondence to:
K. Bergstedt,
kbergste@pppl.gov

Citation:
Bergstedt, K., Ji, H., Jara-Almonte, J., Yoo, J., Ergun, R. E., & Chen, L.-J. (2020). Statistical properties of magnetic structures and energy dissipation during turbulent reconnection in the Earth's magnetotail. *Geophysical Research Letters*, *47*, e2020GL088540. https://doi.org/10.1029/2020GL088540

Received 4 MAY 2020
Accepted 7 SEP 2020
Accepted article online 14 SEP 2020

Abstract We present the first statistical study of magnetic structures and associated energy dissipation observed during a single period of turbulent magnetic reconnection, by using the in situ measurements of the Magnetospheric Multiscale mission in the Earth's magnetotail on 26 July 2017. The structures are selected by identifying a bipolar signature in the magnetic field and categorized as plasmoids or current sheets via an automated algorithm which examines current density and plasma flow. The size of the plasmoids forms a decaying exponential distribution ranging from subelectron up to ion scales. The presence of substantial number of current sheets is consistent with a physical picture of dynamic production and merging of plasmoids during turbulent reconnection. The magnetic structures are locations of significant energy dissipation via electric field parallel to the local magnetic field, while dissipation via perpendicular electric field dominates outside of the structures. Significant energy also returns from particles to fields.

Plain Language Summary Magnetic reconnection is an important mechanism for generating energetic particles in space and solar environments. Turbulent magnetic reconnection causes the development of many small-scale magnetic structures, such as locally helical or loop-like magnetic fields (plasmoids), or areas where oppositely directed magnetic fields are sandwiched together (current sheets). The exact formation and distribution of the structures, as well as the role the structures play in particle energization and the evolution of magnetic reconnection, is still unknown. Using data from the Magnetospheric Multiscale (MMS) mission, we developed an algorithm that is able to detect and identify the magnetic structures present in a region of turbulent magnetic reconnection. The number of structures was found to decrease with size as a decaying exponential, which is consistent with previous theories. The structures contributed strongly to the energization of particles parallel to the local magnetic field, but were not significant sites of energization overall. Overall energization is dominated by energization perpendicular to the local field outside of these structures. There is also significant energy return from particles to the fields.

1. Introduction

Magnetic reconnection is a process by which the topology of the magnetic field within a plasma is altered, allowing for the rapid conversion of magnetic energy into kinetic energy (Parker, 1957). It is responsible for the penetration of solar wind plasma into the magnetosphere (Russell & Elphic, 1978) and plays an important role in powering solar flares and coronal mass ejections (Lin & Forbes, 2000; Sweet, 1969). When reconnecting current sheets are sufficiently stretched to have large aspect ratios, plasmoids are expected to form via the tearing mode instability (Loureiro et al., 2007), leading to the multiscale evolution of fast reconnection (e.g., Bhattacharjee et al., 2009; Shibata & Tanuma, 2001) across space and astrophysics including Earth's magnetotail (Ji & Daughton, 2011). In the latter case, plasmoids have been observed via the ISEE-3 and GEOTAIL satellites over an extended period of time (Baker et al., 1984; Hones Jr et al., 1984; Ieda et al., 1998; Moldwin & Hughes, 1992; Nagai et al., 1994; Richardson et al., 1987; Slavin et al., 2003) and more recently by the CLUSTER mission on the ion scales (e.g., Chen et al., 2008, 2012). Plasmoids are also routinely seen in kinetic simulations (e.g., Daughton et al., 2006; Drake et al., 2006). Therefore, a thorough

analysis of the structures present in a reconnecting current sheet can shed light on the dynamics of fast reconnection, which in turn affect the global dynamics of the magnetosphere.

An important feature of magnetic reconnection is the dissipation of magnetic energy to plasma particle energy through $\boldsymbol{J}\cdot\boldsymbol{E}$ where $\boldsymbol{J}$ and $\boldsymbol{E}$ are current density and electric field, respectively. There is an ongoing debate about whether the component of $\boldsymbol{J}\cdot\boldsymbol{E}$ along or across the local magnetic field, expressed as $J_{\parallel}E_{\parallel}$ and $\boldsymbol{J}_{\perp}\cdot\boldsymbol{E}_{\perp}$, respectively, is the primary source of particle energization (e.g., Drake & Swisdak, 2014; Fox et al., 2018; Pucci et al., 2018; Yamada et al., 2018). Furthermore, whether the dissipation within the localized reconnection structures is significant (e.g., Egedal et al., 2012) or can be ignored (e.g., Drake et al., 2019) in a large system is still unclear. From the same MMS data used in this Letter, Ergun et al. (2018) found that the main positive contributor to the overall $\boldsymbol{J}\cdot\boldsymbol{E}$ was $\boldsymbol{J}_{\perp}\cdot\boldsymbol{E}_{\perp}$ at frequencies at or below the ion cyclotron frequency, but did not examine the spatial correlation between energy dissipation and magnetic structures. Therefore, a detailed statistical study of magnetic dissipation, including the decomposition into parallel and perpendicular components within and outside of the magnetic structures can provide insight on these ongoing debates.

Many analytic and numerical studies have characterized possible size distributions of secondary islands in various regimes (Fermo et al., 2010, 2011; Guo et al., 2013; Huang & Bhattacharjee, 2012; Lingam & Comisso, 2018; Loureiro et al., 2012; Petropoulou et al., 2018; Takamoto, 2013; Uzdensky et al., 2010). Many of these studies have used Magnetohydrodynamic (MHD) models that are not generally applicable to kinetic scale plasmoids. However, the model developed by Fermo et al. (2010) is statistical in nature and therefore can potentially be applied in a multiscale fashion. It postulates that plasmoids start small, then grow in size both by expansion and by plasmoid merging, leading to a smooth energy spectrum via an inverse-cascade (Nakamura et al., 2016). A characteristic of the model of Fermo et al. (2010) is that for sufficiently large size (represented as a characteristic length scale), the number of plasmoids present in a reconnecting current sheet decreases exponentially with increasing plasmoid size. Studies have determined plasmoid size scalings in experimental plasmas (Dorfman et al., 2014; Olson et al., 2016), in solar plasmas via ex situ methods (Guo et al., 2013), and in space plasmas via in situ methods (Akhavan-Tafti et al., 2018; Fermo et al., 2011; Vogt et al., 2014). In situ studies provide more detailed information on each plasmoid, but no in situ study thus far has utilized structures present in only a single turbulently reconnecting region. Plasma conditions varied considerably between each observation and introduced unquantified uncertainties to the observed scaling. An analysis of the distribution of structures within a single turbulently reconnecting current sheet is desirable and necessary for accurately quantifying the plasmoid size scaling.

The most common type of plasmoid observed in the magnetosphere is the flux rope, which is a helical magnetic field structure with a strong core field and an enhancement of the total magnetic field. Flux ropes have been extensively studied in space, and models of cylindrical force-free (Elphic & Russell, 1983) and non-force-free (Lepping et al., 1990; Lundquist, 1950) flux ropes are widely used. Flux ropes have been observed with complex internal structures (Stawarz et al., 2018), including enclosed waves (Wang et al., 2016) and ongoing magnetic reconnection (Øieroset et al., 2016). Various other plasmoids have been observed in the magnetotail current sheet that do not have the typical cylindrical structure, including flattened flux ropes (Sun et al., 2019) and plasmoids which have loop-like field lines rather than helical (Zhang et al., 2013). These nonideal plasmoids are indicative of the dynamic nature of magnetic reconnection. In a turbulent region, plasmoids may experience external forces which could slow or prevent their evolution into ideal cylindrical states. Therefore, for a turbulently reconnecting current sheet, in order to get a comprehensive survey of the plasmoids present, it is necessary to search for plasmoids that do not necessarily fit the ideal cylindrical flux rope model.

Another question for a statistical survey of plasmoids is whether to identify the plasmoids "by eye", or to attempt an automated detection method. Automated methods are more rigorously defined and repeatable, and thus are less susceptible to human sources of bias. For example, methods have been developed to automatically detect flux ropes in satellite data (S. Huang et al., 2018; Smith et al., 2017). These methods are repeatable, rigorous, and calculate valuable parameters such as the spacecraft's distance of closest approach to the center of the flux rope and the flux rope's radius. However, both methods are based on cylindrical flux rope models, force-free (Lundquist, 1950) and non-force-free (Elphic & Russell, 1983), respectively. These methods will not be suitable in a dynamic turbulent reconnection region which is likely to have large numbers of plasmoids which do not fit cylindrical flux rope models and unlikely to have obvious quiescent

magnetic field backgrounds to compare the magnetic field fluctuations against. Therefore, an automated method has been developed to detect nonideal plasmoids, as well as current sheets resulting from two different physical processes. This method has been used to probe the structure, dynamics, and dissipation of a turbulently reconnecting current sheet observed in the magnetotail.

2. Observations and Methodology

MMS observed a period of turbulent reconnection on 26 July 2017 at 07:16:53 UT, and all four satellites collected about 17 min of data at their burst data rates. The electron energization and dissipation during this period was previously studied, and it was found that the main contributor to the overall net positive dissipation was due to $\boldsymbol{J}_\perp \cdot \boldsymbol{E}_\perp$ at or below the ion cyclotron frequency (~0.15 Hz in that region) (Ergun et al., 2018). It was additionally noted that there was a flux-rope-like structure that contained an exceptionally large $J_\parallel E_\parallel$, and that $J_\parallel E_\parallel$ was associated with electrons with energies up to 100 keV. Whether this finding can be generalized to the structures reported here was investigated. For this work, magnetic field data from the Fluxgate Magnetometer (FGM), which has a burst data rate of 128 Hz, is used (Russell et al., 2016). Electric field measurements from the axial and spin-plane double probes at a data rate of 8,192 Hz (Ergun et al., 2016; Lindqvist et al., 2016; Torbert et al., 2016), and electron and ion moments from the Fast Plasma Instrument (FPI) are also used. FPI data are available at burst data resolution of 30 and 150 ms for electrons and ions, respectively (Pollock et al., 2016). The region was characterized by depleted electron and ion densities of $<0.3\,\mathrm{cm}^{-3}$, which led to typical ion and electron inertial lengths of $d_e \sim$ 10–40 km and $d_i \sim$ 400–800 km, respectively. In parts of the turbulent reconnection region, the electron density drops below $0.01\,\mathrm{cm}^{-3}$, which means that the electron moments data will have large uncertainties during those time intervals. We elected not to use the electron moments data in these time intervals.

In order to categorize the structures as plasmoid-like or current sheet-like, idealized two-dimensional models of the structures and their orientations within the magnetotail current sheet were used, as shown in Figure 1. The magnetotail current sheet is generally in the X-Y GSM plane, with the current primarily in the +Y ($J_y > 0$) direction when sufficiently near the Y = 0 plane. Plasmoids will generally be oriented with their invariant directions (e.g., the core direction of a flux rope) in the Y direction, and thus the currents within them will on average be in the +Y direction. We similarly assume that "pull current sheets"—current sheets between plasmoids that are not currently merging—will maintain the same general orientation of the quiescent plasma sheet, and thus be approximately in the X-Y plane, with the current on average in the +Y direction. In contrast, "push current sheets", which are current sheets formed by two plasmoids pushing into each other and potentially merging via reconnection, will be generally oriented in the Y-Z plane. The current direction is opposite that of our model plasmoids, pull current sheets, and the quiescent magnetosphere, so we expect currents within push current sheets to have components in the -Y direction ($J_y < 0$). This distinguishes push current sheets from plasmoids and pull current sheets.

In order to distinguish plasmoids from pull current sheets, we consider the direction of the bipolar signature. This direction will depend on the velocity that the structure is moving with respect to the spacecraft. The characteristic electron and ion speeds in this region are on the order of 100 km/s, whereas the MMS spacecraft are near their apogee and are therefore moving <10 km/s. Therefore, we approximate that the MMS spacecrafts are stationary, and the relevant speed is that of the structures themselves. If the structure has motion in the +X (earthward) direction, a plasmoid will be detected by MMS as a first negative, then positive bipolar B_z signature. In contrast, a pull current sheet will look like a first positive, then negative bipolar signature. If instead the structure is moving in the -X (tailward) direction, a plasmoid will appear as a first positive, the negative bipolar signature, while pull current sheets will appear as first negative, then positive bipolar signatures. Push current sheets will appear as positive-then-negative bipolar signatures if travelling in the +X direction, and negative-then-positive signatures if travelling in the -X direction. This leaves one category of structure without a known physical interpretation (structures with $J_y < 0$ that have a negative-then-positive bipolar signature when travelling in the +X direction), but if the number of events tagged as this category are very small compared to those which have a known physical interpretation, it indicates that the approximate physical interpretations given to the other three categories are good approximations of the physical realities. Using this method, a bipolar B_z structure in the data can be categorized as plasmoid-like, pull-current-sheet-like, or push-current-sheet-like via three considerations: (1) the direction of the bipolar signature (negative-to-positive or positive-to-negative), (2) the direction of the X component of the structure's velocity, and (3) the direction of the Y component of the current density. Structures are

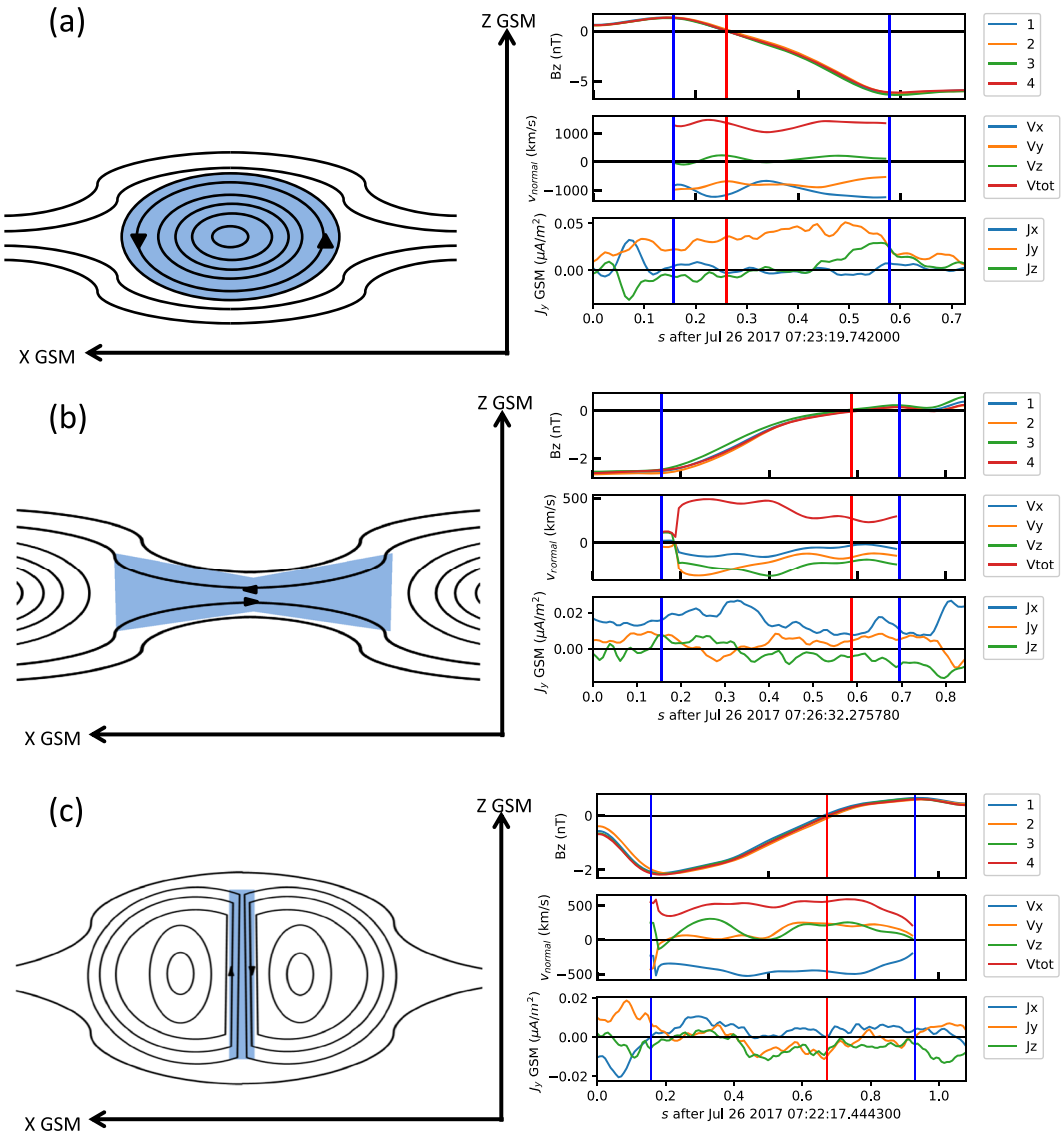

Plasmoids	Pull current sheets	Push current sheets
Vx positive (negative)	Vx postive (negative)	Vx positive (negative)
Jy GSM positive	Jy GSM positive	Jy GSM negative
Bz bipolar increasing (decreasing)	Bz bipolar decreasing (increasing)	Bz bipolar decreasing (increasing)

Figure 1. Left- cartoon model of the structure categories. Right- example of a structure from data. For (a) a tailward-moving plasmoid, (b) a tailward-moving pull current sheet, (c) a tailward-moving push current sheet. The red vertical bar denotes the zero crossing and the blue bars denote the beginning and end of the structure. The magnetic field data were smoothed by a six-point Hamming window for better estimation of the structure durations. Table: A summary of the selection criteria for the three structure categories.

hereafter referred to as "plasmoids", "pull current sheets", or "push current sheets" depending on their categorization in this manner. Examples of these three types of structures are shown on the right side of Figure 1, and a summary of the selection criteria is in the table at the bottom of that figure.

Structure candidates were first selected by identifying their bipolar B_z signature in MMS1. In order to avoid some of the high-frequency transient turbulent magnetic field fluctuations, the data were first smoothed

with a six-point Hamming window. Upon finding potential structure candidates, their sizes were determined by finding the nearest local minimum in the negative part of the bipolar signature, and the nearest local maxima in the positive part of the bipolar signature. The number of comparison points for determining a local extrema was variable, but for the primary data, 10 points to each side were used. At this point, if the other MMS satellites did not also observe a bipolar B_z signature within the structure candidate, the structure candidate was discarded. The magnetic field data for the structure were then synced to a common timeline via a four-point Bartlett window (Harvey & Schwartz, 1998), and the lower resolution ion and electron moments data were synced to the same timeline via a cubic spline interpolation. The electric field data were synced to a common timeline via a linear interpolation to avoid artificial oscillations.

In order to calculate the structures' velocities and current densities, multispacecraft techniques were used. The current density was calculated via the curlometer technique (Dunlop et al., 2002; Robert et al., 1998). The structure velocity was calculated in a two-step process. First, the dimensionality, invariant directions, and natural coordinates of the structure were calculated using the Minimum Directional Derivative (MDD) technique (Shi et al., 2005), using the linear approximation of the magnetic field spatial gradient tensor from the barycentric coordinate approach (Chanteur, 1998). Then the Spatio-Temporal difference (STD) method was applied to determine the velocity of the structure in its noninvariant directions (Shi et al., 2006). The STD method cannot be used to determine the structure's velocity in its invariant directions (e.g., the core direction of an ideal flux rope), but motion in these directions by definition does not cause a large change of the magnetic field strength or direction. Therefore, the velocity in the noninvariant directions is sufficient to determine the structure's general motion in the X direction for categorization purposes.

There are some additional limitations to the multispacecraft techniques used. For one, they are only reliable when all four spacecraft of the tetrahedron are within the same structure. The spacecraft spacing was ~11 km during this interval, while the electron skin depth was ~15–20 km, so the multispacecraft techniques would be unreliable for subelectron-scale structures. The tetrahedron also must have a Tetrahedron Quality Factor (TQF) of greater than 0.7 (Fuselier et al., 2016), which was satisfied during the interval. The techniques also assume approximate time stationarity, so any temporal fluctuations caused by the turbulence in the region could systematically affect the results from MDD and STD. The techniques also have some advantages; namely, they can be used at every data point in the time cadence, unlike other techniques that determine natural coordinates for structures such as minimum-variance analysis which can be used on data from a single spacecraft (Sonnerup & Cahill Jr., 1967; Sonnerup & Scheible, 1998). This also allowed us to evaluate the time-stationarity of the data by observing how the results from MDD and STD change with time throughout the structure.

3. Statistical Results

3.1. Magnetic Structure Properties

There were 288 structures observed, and a summary of them is shown in Figure 2. Of these, 94 were plasmoids, 99 were pull current sheets, and 51 were push current sheets. Thirty-four structures could not be categorized due to low certainty in the overall direction of the X component of the velocity or the Y component of the current density. Ten had sufficient certainty to be categorized, but did not match any of the given categories. These accounted for ~3% of the identified structures, so we conclude that the categories devised were adequate to describe the majority of sufficiently certain cases. Statistics were then performed on each of the structure types separately.

An attempt was made to fit the observed plasmoids to force-free and non-force-free flux rope models in order to accurately measure the plasmoids' radii; however, the fits were inconclusive. Therefore, each structure's size was approximated by the product of the normal velocity of the structure and the duration of the structure. By this method, the majority of the structures were $<10d_e$ in size, electron-scale. The size distribution histograms of plasmoids and pull current sheets are shown in Figure 2. The size data for plasmoids and pull current sheets were fit using maximum likelihood estimation (MLE), which does not require binning the data and is therefore more robust. Kolmogorov-Smirnov testing of the fits (Chakravarti et al., 1967) found consistency with an exponential distribution but not with a power law. The push current sheets did not have a definitive fit (not shown). This decaying exponential is consistent with the prediction of Fermo et al. (2010) for sufficiently large scale size. This is the first in situ confirmation of Fermo et al.'s prediction from observations taken from a single turbulently reconnecting region.

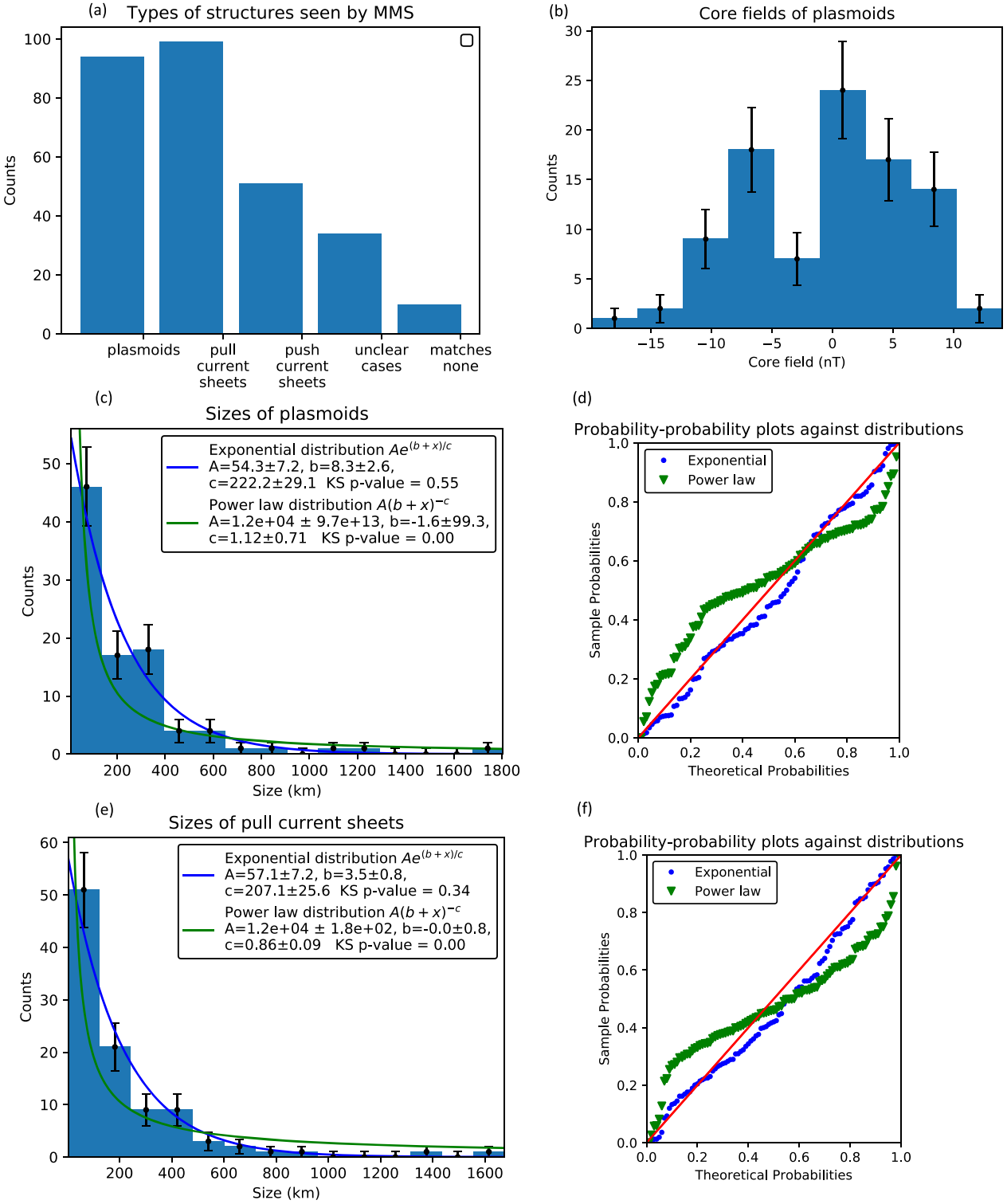

Figure 2. (a) Summary bar chart of structure types counted. (b) Histogram of the averaged core fields of the observed plasmoids. (c) Histogram of plasmoid sizes. (d) Probability-probability plot of the exponential and power law fits for the plasmoid size data. (e) Histogram of pull current sheet sizes. (f) Probability-probability plot of the exponential and power law fits for the pull current sheet size data. Error bars are from Poisson uncertainties. The errors on the fit parameters were computed by $n = 100$ bootstrap using (Pedregosa et al., 2011). Kolmogorov-Smirnov tests (Chakravarti et al., 1967) were performed on the exponential and power law fits, which accepted the exponential fit and rejected the power law fit. The probability-probability plots for the power law fits were done using a truncated power law distribution, as our selection mechanism is only sensitive to structures of a particular size range. Typical electron and ion inertial lengths of $d_e \sim 10$–40 km and $d_i \sim 400$–800 km, respectively show the given structures range from a few electron to a few ion inertial lengths in size.

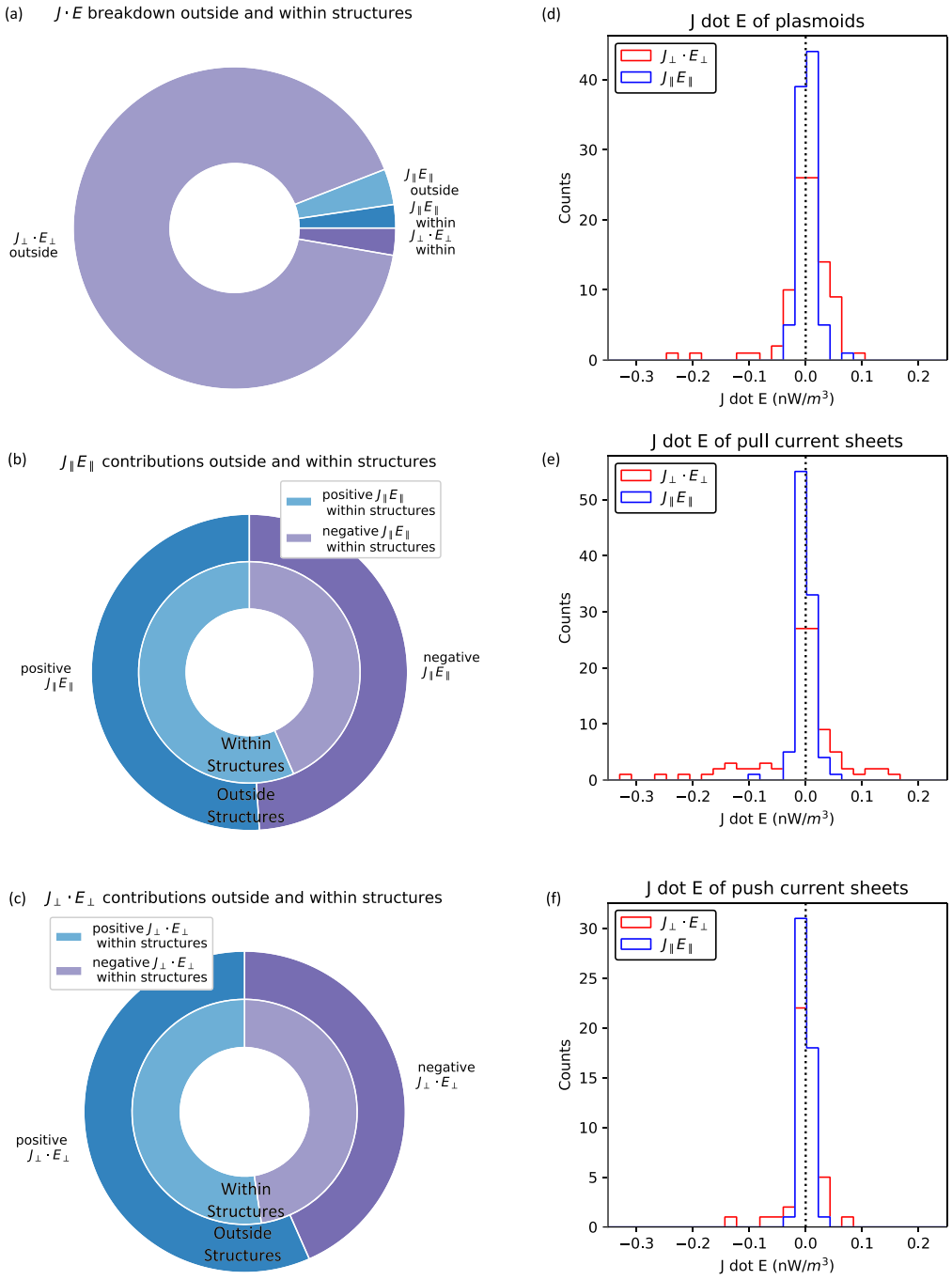

Figure 3. (a) Breakdown of the net contribution to $J_\parallel E_\parallel$ and $\boldsymbol{J}_\perp \cdot \boldsymbol{E}_\perp$ from the structures, compared to the regions outside the structures. (b) Comparison of the positive and negative contributions to $J_\parallel E_\parallel$. Outside circle is contributions from outside the structures, inside circle is contributions from the structures. (c) Comparison of the positive and negative contributions to $\boldsymbol{J}_\perp \cdot \boldsymbol{E}_\perp$. Outside circle is contributions from outside the structures, inside circle is contributions from the structures. (d–f) Histogram comparing the averaged contributions of magnetic structures to $J_\parallel E_\parallel$ and $\boldsymbol{J}_\perp \cdot \boldsymbol{E}_\perp$ for (d) plasmoids, (e) pull current sheets, and (f) push current sheets.

Due to the turbulent nature of the magnetic field, we did not calculate the overall guide field of the reconnecting region. The guide field during magnetotail reconnection can change significantly on the timescale of less than a minute, so this event may not have a consistent overall guide field (Chen et al., 2019). Instead, we calculated the core fields of the observed plasmoids by finding the magnetic field strength along the most invariant direction determined from MDD analysis. This most invariant direction was generally primarily aligned with the GSM Y direction, so the distribution of the core fields of the plasmoids will be indicative of the total guide field of the region. Figure 2 shows the distribution of observed core fields of the plasmoids, with positive core fields being aligned with the +Y GSM direction and negative core fields aligned with the -Y GSM direction. There are more plasmoids with positive core fields than negative ones, indicating a possible slight positive guide field. However, the core fields are not overwhelmingly in the +Y direction, indicating that the guide field was not strong, or was changing over the course of the event. In the case of stronger guide field, it would be possible to follow the procedure outlined by Nakamura et al. (2016) to use band-pass filtering to identify electron-scale flux ropes. However, for weak guide field the structures identified in this fashion may be the product of instabilities other than the tearing instability, and therefore the technique is not appropriate for these data.

3.2. Particle Energization and Dissipation

To determine the dissipation mechanisms of the structures, we compared the $J_{\parallel}E_{\parallel}$ and $\boldsymbol{J}_{\perp}\cdot\boldsymbol{E}_{\perp}$ contributions from the structures and from outside the structures, summarized in the pie chart in Figure 3. The structures covered ∼10% of the total time duration of the region, but they contributed ∼40% of the total $J_{\parallel}E_{\parallel}$ and only ∼3% of the total $\boldsymbol{J}_{\perp}\cdot\boldsymbol{E}_{\perp}$. These electron-to-ion-scale structures are major contributors to the $J_{\parallel}E_{\parallel}$ in the region, which is consistent with Ergun et al. (2018)'s identification of a flux-rope-like structure associated with large $J_{\parallel}E_{\parallel}$ and highly energized electrons of >100 keV. However, the breakdown between positive and negative contributions to $\boldsymbol{J}\cdot\boldsymbol{E}$ shows more complexity. As shown in Figure 3, the regions both inside and outside of the structures have significant positive and negative contributions to $J_{\parallel}E_{\parallel}$ and $\boldsymbol{J}_{\perp}\cdot\boldsymbol{E}_{\perp}$. The structures have a larger ratio of positive to negative for $J_{\parallel}E_{\parallel}$, leading to their significant contribution to net $J_{\parallel}E_{\parallel}>0$. In contrast, the region outside of the structures has a larger ratio of positive to negative for $\boldsymbol{J}_{\perp}\cdot\boldsymbol{E}_{\perp}$, leading to a much smaller contribution from the structures, which are closer to parity. This breakdown shows that both within and outside of the structures, there is ongoing energy conversion from fields to particles and vice versa, whereas the net energy exchange favors particle energization.

The histograms of the averaged $J_{\parallel}E_{\parallel}$ and $\boldsymbol{J}_{\perp}\cdot\boldsymbol{E}_{\perp}$ are shown for the three major structure types in Figure 3, and they confirm that the structures are sources of both positive and negative $\boldsymbol{J}\cdot\boldsymbol{E}$. The average perpendicular components have a larger spread than the parallel components by a factor of ∼2, indicating that $\boldsymbol{J}_{\perp}\cdot\boldsymbol{E}_{\perp}$ has the larger impact on overall $\boldsymbol{J}\cdot\boldsymbol{E}$, whether positive or negative. The histograms for the plasmoids show a bias towards positive $\boldsymbol{J}\cdot\boldsymbol{E}$, both for the parallel and perpendicular components, indicating these structures are on average sites of some particle acceleration. There are some notable outliers, but they do not significantly impact the structures' average contributions.

Overall, $\boldsymbol{J}_{\perp}\cdot\boldsymbol{E}_{\perp}$ contributes ∼90% of the total $\boldsymbol{J}\cdot\boldsymbol{E}$, whereas $J_{\parallel}E_{\parallel}$ only accounts for ∼10%, and ∼85% of the total average $\boldsymbol{J}\cdot\boldsymbol{E}$ comes from $\boldsymbol{J}_{\perp}\cdot\boldsymbol{E}_{\perp}$ outside of the structures. Therefore, the structures have a small contribution to the overall $\boldsymbol{J}\cdot\boldsymbol{E}$, though some may serve as injection sites with large $J_{\parallel}E_{\parallel}$ which provide rapid energization to small populations of electrons, while the $\boldsymbol{J}_{\perp}\cdot\boldsymbol{E}_{\perp}$ between structures provides the largest net energization, such as proposed in Comisso and Sironi (2019). This result supports the use of codes which simulate particle energization during magnetic reconnection on larger-than-kinetic scales, such as the one detailed in Drake et al. (2019), but some handling of electron injection source terms may still be necessary.

4. Conclusions and Discussion

We utilized two-dimensional models of the expected magnetic signatures of plasmoids, pull current sheets, and push current sheets to automate the detection and categorization of 288 magnetic structures within a 17-min turbulent reconnection region. The majority of these had sizes between the electron and ion skin depths, making this the first statistical survey of mainly electron-scale structures within the same current sheet. It is possible to change the parameters of the detection algorithm to find systematically larger structures, but the focus of this work was on the smaller-scale ones, which may potentially be embedded within larger structures.

The estimated size distribution of the plasmoids was found to fit a decaying exponential, which is consistent with Fermo et al. (2010)'s statistical model of plasmoid distribution, growth, and merging. The presence of push current sheets consistent with plasmoid merging provides further evidence of the importance of merging plasmoid dynamics to the overall structure of the reconnecting current sheet. The bulk motion of the structures supports the analysis of Ergun et al. (2018), who observed a large-scale reconnection region with turbulent outflows. We also noticed that structure sizes were positively correlated with the structure speeds (not shown). However, the resolution limit of the magnetic field data prevents detection of small, fast-moving structures. Additionally, structure speed is used to calculate size, so there could be some artificial correlation.

The region was shown to have significant energy conversion from fields to particles and vice versa, but net $\boldsymbol{J}\cdot\boldsymbol{E}$ was positive for particle energization at the expense of the field energy. On average the structures were significant contributors to the net $J_{\parallel}E_{\parallel}$ of the region, contributing ~40% of the net $J_{\parallel}E_{\parallel}$. In contrast, 97% of the $\boldsymbol{J}_{\perp}\cdot\boldsymbol{E}_{\perp}$ contribution was from the regions between the structures, meaning that these larger regions were the main contributor to the overall positive $J\cdot E$, which was composed of 85% $\boldsymbol{J}_{\perp}\cdot\boldsymbol{E}_{\perp}$ from outside of the structures. This is consistent with a model of the structures as injection sites, with strong localized $J_{\parallel}E_{\parallel}$ able to quickly accelerate electrons, which then can be slowly accelerated along with ions in the larger-scale regions of net positive $\boldsymbol{J}_{\perp}\cdot\boldsymbol{E}_{\perp}$. This indicates that the majority of the particle acceleration from these turbulent reconnection regions can be modeled using larger-scale physics, with the smaller-scale $J_{\parallel}E_{\parallel}$ injection sites largely ignored, or modeled as source terms of energetic electrons. Therefore, codes which are focused on capturing the larger-scale dynamics of reconnection regions (such as Drake et al., 2019), perhaps with added electron injection, should accurately describe the bulk of the particle energization in the reconnection region.

Fitting the plasmoids to mathematical models would yield more details about their structure. We found that the observed plasmoids did not fit the constraints of force-free or non-force free cylindrical models, but more general models were not tried. The use of other methods for ascertaining magnetic field topology, such as the first-order Taylor expansion method outlined in Fu et al. (2015), would also provide greater insight into the structure of this turbulently reconnecting region.

It would be valuable to repeat the analysis of this paper using a different plasmoid detection algorithm, such as the method detailed in Nakamura et al. (2016), which requires strong guide field. A machine learning algorithm could possibly be more comprehensive than our algorithm, which has inflexible cutoffs for structure detection. This work did not explore whether the observed current sheets were reconnecting or not. If a nuanced automated method was developed to detect evidence of ongoing reconnection, additional information about the dynamics of the reconnection region could be obtained.

Another valuable expansion of this work would be to examine particular structures of interest from a three-dimensional viewpoint. Recent works such as Øieroset et al. (2016, 2019) have shown that structures which fit simple two-dimensional models such as that of a flux rope can have more complex three-dimensional topology, which can impact the onset and rate of reconnection. Given the large number of magnetic structures and potential for multiple X-line reconnection in this region, an in-depth three-dimensional exploration of even a few of the magnetic structures in this region has the potential to provide further insight into turbulent reconnection dynamics.

Data Availability Statement

The data used are available from the MMS Science Data center (https://lasp.colorado.edu/mms/sdc/public/). Analysis scripts used for this manuscript can be found in the DataSpace of Princeton University (https://dataspace.princeton.edu/handle/88435/dsp01x920g025r).

Acknowledgments
This work was supported by the U.S. Department of Energy's Office of Fusion Energy Sciences under Contract No. DE-AC0209CH11466, by NASA under Grant No. NNH15AB29I, and by the National Science Foundation Graduate Research Fellowship under Grant No. DGE-2039656. Any opinions, findings, and conclusions or recommendations expressed in this material are those of the authors and do not necessarily reflect the views of the funding organizations.

References

Akhavan-Tafti, M., Slavin, J. A., Le, G., Eastwood, J. P., Strangeway, R. J., Russell, C. T., et al. (2018). Mms examination of ftes at the earth's subsolar magnetopause. *Journal of Geophysical Research: Space Physics*, *123*, 1224–1241. https://doi.org/10.1002/2017JA024681

Baker, D. N., Bame, S. J., Birn, J., Feldman, W. C., Gosling, J. T., Hones Jr., E. W., et al. (1984). Direct observations of passages of the distant neutral line (80-140 re) following substorm onsets: Isee-3. *Geophysical Research Letters*, *11*(10), 1042–1045. https://doi.org/10.1029/GL011i010p01042

Bhattacharjee, A., Huang, Y. M., Yang, H., & Rogers, B. (2009). Fast reconnection in high-lundquist-number plasmas due to the plasmoid instability. *Physics of Plasmas*, *16*, 112102.
Chakravarti, I. M., Laha, R. G., & Roy, J. (1967). *Handbook of methods of applied statistics, volume i*. New York: John Wiley and Sons.
Chanteur, G. (1998). Spatial interpolation for four spacecraft: Theory. In G. Paschmann & P. W. Daly (Eds.), *Analysis methods for multi-spacecraft data* (pp. 349–370). Switzerland: International Space Science Institute.
Chen, L. J., Bhattacharjee, A., Puhl-Quinn, P. A., Yang, H., Bessho, N., Imada, S., et al. (2008). Observation of energetic electrons within magnetic islands. *Nature Physics*, *4*(1), 19–23. https://doi.org/10.1038/nphys777
Chen, L.-J., Daughton, W., Bhattacharjee, A., Torbert, R. B., Roytershteyn, V., & Bessho, N. (2012). In-plane electric fields in magnetic islands during collisionless magnetic reconnection. *Physics of Plasmas*, *19*(11), 112902. https://doi.org/10.1063/1.4767645
Chen, L.-J., Wang, S., Hesse, M., Ergun, R. E., Moore, T., Giles, B., et al. (2019). Electron diffusion regions in magnetotail reconnection under varying guide fields. *Geophysical Research Letters*, *46*, 6230–6238. https://doi.org/10.1029/2019GL082393
Comisso, L., & Sironi, L. (2019). The interplay of magnetically dominated turbulence and magnetic reconnection in producing nonthermal particles. *The Astrophysical Journal*, *886*(2), 122. https://doi.org/10.3847/1538-4357/ab4c33
Daughton, W., Scudder, J., & Karimabadi, H. (2006). Fully kinetic simulations of undriven magnetic reconnection with open boundary conditions. *Physical of Plasmas*, *13*, 072101.
Dorfman, S., Ji, H., Yamada, M., Yoo, J., Lawrence, E., Myers, C., & Tharp, T. D. (2014). Experimental observation of 3-d, impulsive reconnection events in a laboratory plasma. *Physics of Plasmas*, *21*(1), 012109. https://doi.org/10.1063/1.4862039
Drake, J. F., Arnold, H., Swisdak, M., & Dahlin, J. T. (2019). A computational model for exploring particle acceleration during reconnection in macroscale systems. *Physics of Plasmas*, *26*(1), 012901. https://doi.org/10.1063/1.5058140
Drake, J. F., & Swisdak, M. (2014). The onset of ion heating during magnetic reconnection with a strong guide field. *Physics of Plasmas*, *21*(7), 072903. https://doi.org/10.1063/1.4889871
Drake, J. F., Swisdak, M., Schoeffler, K. M., Rogers, B. N., & Kobayashi, S. (2006). Formation of secondary islands during magnetic reconnection. *Geophysical Research Letters*, *33*, L13105. https://doi.org/10.1029/2006GL025957
Dunlop, M. W., Balogh, A., Glassmeier, K.-H., & Robert, P. (2002). Four-point cluster application of magnetic field analysis tools: The curlometer. *Journal of Geophysical Research*, *107*(A11), SMP 23–1–SMP 23–14. https://doi.org/10.1029/2001JA005088
Egedal, J., Daughton, W., & Le, A. (2012). Large-scale electron acceleration by parallel electric fields during magnetic reconnection. *Nature Physics*, *8*, 321–324.
Elphic, R. C., & Russell, C. T. (1983). Magnetic flux ropes in the venus ionosphere: Observations and models. *Journal of Geophysical Research*, *88*(A1), 58–72. https://doi.org/10.1029/JA088iA01p00058
Ergun, R. E., Goodrich, K. A., Wilder, F. D., Ahmadi, N., Holmes, J. C., Eriksson, S., et al. (2018). Magnetic reconnection, turbulence, and particle acceleration: Observations in the earth's magnetotail. *Geophysical Research Letters*, *45*, 3338–3347. https://doi.org/10.1002/2018GL076993
Ergun, R. E., Tucker, S., Westfall, J., Goodrich, K. A., Malaspina, D. M., Summers, D., et al. (2016). The axial double probe and fields signal processing for the mms mission. *Space Science Reviews*, *199*(1), 167–188. https://doi.org/10.1007/s11214-014-0115-x
Fermo, R. L., Drake, J. F., & Swisdak, M. (2010). A statistical model of magnetic islands in a current layer. *Physical of Plasmas*, *17*(1), 010702.
Fermo, R. L., Drake, J. F., Swisdak, M., & Hwang, K.-J. (2011). Comparison of a statistical model for magnetic islands in large current layers with Hall MHD simulations and Cluster FTE observations. *Journal of Geophysical Research*, *116*, A09226. https://doi.org/10.1029/2010JA016271
Fox, W., Wilder, F. D., Eriksson, S., Jara-Almonte, J., Pucci, F., Yoo, J., et al. (2018). Energy conversion by parallel electric fields in reconnection diffusion regions in scaled laboratory and space experiments. *Geophysical Research Letters*, *45*, 12,677–12,684. https://doi.org/10.1029/2018GL079883
Fu, H. S., Vaivads, A., Khotyaintsev, Y. V., Olshevsky, V., Andr, M., Cao, J. B., et al. (2015). How to find magnetic nulls and reconstruct field topology with mms data *Journal of Geophysical Research: Space Physics*, *120*, 3758–3782. https://doi.org/10.1002/2015JA021082
Fuselier, S. A., Lewis, W. S., Schiff, C., Ergun, R., Burch, J. L., Petrinec, S. M., & Trattner, K. J. (2016). Magnetospheric multiscale science mission profile and operations. *Space Science Reviews*, *199*(1–4), 77–103. https://doi.org/10.1007/s11214-014-0087-x
Guo, L.-J., Bhattacharjee, A., & Huang, Y.-M. (2013). Distribution of plasmoids in post-coronal mass ejection current sheets. *The Astrophysical Journal Letters*, *771*, L14.
Harvey, C. C., & Schwartz, S. J. (1998). Time series resampling methods. In G. Paschmann & P. W. Daly (Eds.), *Analysis methods for multi-spacecraft data* (pp. 43–64). Switzerland: International Space Science Institute.
Hones Jr, E. W., Baker, D. N., Bame, S. J., Feldman, W. C., Gosling, J. T., McComas, D. J., et al. (1984). Structure of the magnetotail at 220 re and its response to geomagnetic activity. *Geophysical Research Letters*, *11*(1), 5–7.
Huang, Y.-M., & Bhattacharjee, A. (2012). Distribution of plasmoids in high-lundquist-number magnetic reconnection. *Physical Review Letters*, *109*(26), 265002.
Huang, S., Zhao, P., He, J., Yuan, Z., Zhou, M., Fu, H., et al. (2018). A new method to identify flux ropes in space plasmas. *Annales Geophysicae*, *36*(5), 1275–1283. https://doi.org/10.5194/angeo-36-1275-2018
Ieda, A., Machida, S., Mukai, T., Saito, Y., Yamamoto, T., Nishida, A., et al. (1998). Statistical analysis of the plasmoid evolution with geotail observations. *Journal of Geophysical Research*, *103*(A3), 4453–4465. https://doi.org/10.1029/97JA03240
Ji, H., & Daughton, W. (2011). Phase diagram for magnetic reconnection in heliophysical, astrophysical, and laboratory plasmas. *Physical of Plasmas*, *18*(11), 111207.
Lepping, R. P., Jones, J. A., & Burlaga, L. F. (1990). Magnetic field structure of interplanetary magnetic clouds at 1 au. *Journal of Geophysical Research*, *95*(A8), 11,957–11,965. https://doi.org/10.1029/JA095iA08p11957
Lin, J., & Forbes, T. G. (2000). Effects of reconnection on the coronal mass ejection process. *Journal of Geophysical Research*, *105*(A2), 2375–2392. https://doi.org/10.1029/1999JA900477
Lindqvist, P.-A., Olsson, G., Torbert, R. B., King, B., Granoff, M., Rau, D., et al. (2016). The spin-plane double probe electric field instrument for mms. *Space Science Reviews*, *199*(1), 137–165. https://doi.org/10.1007/s11214-014-0116-9
Lingam, M., & Comisso, L. (2018). A maximum entropy principle for inferring the distribution of 3d plasmoids. *Physics of Plasmas*, *25*(1), 012114. https://doi.org/10.1063/1.5020887
Loureiro, N. F., Samtaney, R., Schekochihin, A. A., & Uzdensky, D. A. (2012). Magnetic reconnection and stochastic plasmoid chains in high-lundquist-number plasmas. *Physics of Plasmas*, *19*(4), 042303. https://doi.org/10.1063/1.3703318
Loureiro, N. F., Schekochihin, A. A., & Cowley, S. C. (2007). Instability of current sheets and formation of plasmoid chains. *Physical of Plasmas*, *14*, 100703.
Lundquist, S. (1950). Magneto-hydrostatic fields. *Arkiv för fysik*, *2*, 361–365.

Moldwin, M. B., & Hughes, W. J. (1992). On the formation and evolution of plasmoids: A survey of isee 3 geotail data. *Journal of Geophysical Research*, *97*(A12), 19,259–19,282. https://doi.org/10.1029/92JA01598

Nagai, T., Takahashi, K., Kawano, H., Yamamoto, T., Kokubun, S., & Nishida, A. (1994). Initial geotail survey of magnetic substorm signatures in the magnetotail. *Geophysical Research Letters*, *21*(25), 2991–2994. https://doi.org/10.1029/94GL01420

Nakamura, T. K. M., Nakamura, R., Narita, Y., Baumjohann, W., & Daughton, W. (2016). Multi-scale structures of turbulent magnetic reconnection. *Physics of Plasmas*, *23*(5), 052116. https://doi.org/10.1063/1.4951025

Øieroset, M., Phan, T. D., Drake, J. F., Eastwood, J. P., Fuselier, S. A., Strangeway, R. J., et al. (2019). Reconnection with magnetic flux pileup at the interface of converging jets at the magnetopause. *Geophysical Research Letters*, *46*, 1937–1946. https://doi.org/10.1029/2018GL080994

Øieroset, M., Phan, T. D., Haggerty, C., Shay, M. A., Eastwood, J. P., Gershman, D. J., et al. (2016). MMS observations of large guide field symmetric reconnection between colliding reconnection jets at the center of a magnetic flux rope at the magnetopause. *Geophysical Research Letters*, *43*, 5536–5544. https://doi.org/10.1002/2016GL069166

Olson, J., Egedal, J., Greess, S., Myers, R., Clark, M., Endrizzi, D., et al. (2016). Experimental demonstration of the collisionless plasmoid instability below the ion kinetic scale during magnetic reconnection. *Physical Review Letters*, *116*(25), 255001.

Parker, E. N. (1957). Sweet's mechanism for merging magnetic fields in conducting fluids. *Journal of Geophysical Research*, *62*, 509.

Pedregosa, F., Varoquaux, G., Gramfort, A., Michel, V., Thirion, B., Grisel, O., et al. (2011). Scikit-learn: Machine learning in Python. *Journal of Machine Learning Research*, *12*, 2825–2830.

Petropoulou, M., Christie, I. M., Sironi, L., & Giannios, D. (2018). Plasmoid statistics in relativistic magnetic reconnection. *Monthly Notices of the Royal Astronomical Society*, *475*(3), 3797–3812. https://doi.org/10.1093/mnras/sty033

Pollock, C., Moore, T., Jacques, A., Burch, J., Gliese, U., Saito, Y., et al. (2016). Fast plasma investigation for magnetospheric multiscale. *Space Science Reviews*, *199*(1–4), 331–406.

Pucci, F., Usami, S., Ji, H., Guo, X., Horiuchi, R., Okamura, S., et al. (2018). Energy transfer and electron energization in collisionless magnetic reconnection for different guide-field intensities. *Physics of Plasmas*, *25*(12), 122111. https://doi.org/10.1063/1.5050992

Richardson, I. G., Cowley, S. W. H., Hones Jr., E. W., & Bame, S. J. (1987). Plasmoid-associated energetic ion bursts in the deep geomagnetic tail: Properties of plasmoids and the postplasmoid plasma sheet. *Journal of Geophysical Research*, *92*(A9), 9997–10,013. https://doi.org/10.1029/JA092iA09p09997

Robert, P., Dunlop, M. W., Roux, A., & Chanteur, G. (1998). Accuracy of current density determination. In G. Paschmann & P. W. Daly (Eds.), *Analysis methods for multi-spacecraft data* (pp. 395–418). Switzerland: International Space Science Institute.

Russell, C. T., Anderson, B. J., Baumjohann, W., Bromund, K. R., Dearborn, D., Fischer, D., et al. (2016). The magnetospheric multiscale magnetometers. *Space Science Reviews*, *199*(1–4), 189–256.

Russell, C. T., & Elphic, R. C. (1978). Initial ISEE Magnetometer Results: Magnetopause Observations (Article published in the special issues: Advances in Magnetospheric Physics with GEOS- 1 and ISEE - 1 and 2.). *Space Science Reviews*, *22*(6), 681–715.

Shi, Q. Q., Shen, C., Dunlop, M. W., Pu, Z. Y., Zong, Q.-G., Liu, Z. X., et al. (2006). Motion of observed structures calculated from multi-point magnetic field measurements: Application to cluster. *Geophysical Research Letters*, *33*, L08109. https://doi.org/10.1029/2005GL025073

Shi, Q. Q., Shen, C., Pu, Z. Y., Dunlop, M. W., Zong, Q.-G., Zhang, H., et al. (2005). Dimensional analysis of observed structures using multipoint magnetic field measurements: Application to cluster. *Geophysical Research Letters*, *32*, L12105. https://doi.org/10.1029/2005GL022454

Shibata, K., & Tanuma, S. (2001). Plasmoid-induced-reconnection and fractal reconnection. *Earth Planets Space*, *53*, 473.

Slavin, J. A., Lepping, R. P., Gjerloev, J., Fairfield, D. H., Hesse, M., Owen, C. J., et al. (2003). Geotail observations of magnetic flux ropes in the plasma sheet. *Journal of Geophysical Research*, *108*(A1), SMP 10–1–SMP 10–18. https://doi.org/10.1029/2002JA009557

Smith, A. W., Slavin, J. A., Jackman, C. M., Fear, R. C., Poh, G.-K., DiBraccio, G. A., et al. (2017). Automated force-free flux rope identification. *Journal of Geophysical Research: Space Physics*, *122*, 780–791. https://doi.org/10.1002/2016JA022994

Sonnerup, B. U. O., & Cahill Jr., L. J. (1967). Magnetopause structure and attitude from explorer 12 observations. *Journal of Geophysical Research*, *72*(1), 171–183. https://doi.org/10.1029/JZ072i001p00171

Sonnerup, B. U. O., & Scheible, M. (1998). Minimum and maximum variance analysis. In G. Paschmann & P. W. Daly (Eds.), *Analysis methods for multi-spacecraft data* (pp. 185–220). Switzerland: International Space Science Institute.

Stawarz, J. E., Eastwood, J. P., Genestreti, K. J., Nakamura, R., Ergun, R. E., Burgess, D., et al. (2018). Intense electric fields and electron-scale substructure within magnetotail flux ropes as revealed by the magnetospheric multiscale mission. *Geophysical Research Letters*, *45*, 8783–8792. https://doi.org/10.1029/2018GL079095

Sun, W. J., Slavin, J. A., Tian, A. M., Bai, S. C., Poh, G. K., Akhavan-Tafti, M., et al. (2019). Mms study of the structure of ion-scale flux ropes in the earth's cross-tail current sheet. *Geophysical Research Letters*, *46*, 6168–6177. https://doi.org/10.1029/2019GL083301

Sweet, P. A. (1969). Mechanisms of solar flares. *Annual Review of Astronomy and Astrophysics*, *7*(1), 149–176. https://doi.org/10.1146/annurev.aa.07.090169.001053

Takamoto, M. (2013). Evolution of relativistic plasmoid chains in a poynting-dominated plasma. *The Astrophysical Journal*, *775*(1), 50. https://doi.org/10.1088/0004-637X/775/1/50

Torbert, R. B., Russell, C. T., Magnes, W., Ergun, R. E., Lindqvist, P.-A., LeContel, O., et al. (2016). The fields instrument suite on mms: Scientific objectives, measurements, and data products. *Space Science Reviews*, *199*(1), 105–135. https://doi.org/10.1007/s11214-014-0109-8

Uzdensky, D. A., Loureiro, N. F., & Schekochihin, A. A. (2010). Fast magnetic reconnection in the plasmoid-dominated regime. *Physical Review Letters*, *105*, 235002. https://doi.org/10.1103/PhysRevLett.105.235002

Vogt, M. F., Jackman, C. M., Slavin, J. A., Bunce, E. J., Cowley, S. W. H., Kivelson, M. G., & Khurana, K. K. (2014). Structure and statistical properties of plasmoids in jupiter's magnetotail. *Journal of Geophysical Research: Space Physics*, *119*, 821–843. https://doi.org/10.1002/2013JA019393

Wang, R., Lu, Q., Nakamura, R., Huang, C., Li, X., Wu, M., et al. (2016). Electrostatic and electromagnetic fluctuations detected inside magnetic flux ropes during magnetic reconnection. *Journal of Geophysical Research: Space Physics*, *121*, 9473–9482. https://doi.org/10.1002/2016JA022906

Yamada, M., Chen, L. J., Yoo, J., Wang, S., Fox, W., Jara-Almonte, J., et al. (2018). The two-fluid dynamics and energetics of the asymmetric magnetic reconnection in laboratory and space plasmas. *Nature Communications*, *9*, 5223.

Zhang, Y. C., Shen, C., Liu, Z. X., Rong, Z. J., Zhang, T. L., Marchaudon, A., et al. (2013). Two different types of plasmoids in the plasma sheet: Cluster multisatellite analysis application. *Journal of Geophysical Research: Space Physics*, *118*, 5437–5444. https://doi.org/10.1002/jgra.50542